

Implementation of KrF DBARCs for implant applications on advanced lithography nodes

Joyce Lowes^a, Alice Guerrero^a, Michael Weigand^a, Carlton Washburn^a, Charlyn Stroud^a, Shalini Sharma^b, David Torres^b, Mark Slezak^b, Gary Dabbagh^b, Cherry Tang^b

^aBrewer Science, Inc., 2401 Brewer Drive, Rolla, MO 65401, USA

^bJSR Micro, Inc., 1280 North Mathilda Avenue, Sunnyvale, CA, 94089, USA

ABSTRACT

Traditional implant layers are becoming increasingly complex in design and continuously pushing resolution limits lower. In response, developer-soluble bottom anti-reflective coatings (DBARCs) were introduced to meet these more challenging requirements. These DBARCs excelled over the traditional combination of single-layer resist and dyed resist/top anti-reflective coating (TARC). DBARCs offered the resolution and critical dimension (CD) control needed for the increasingly critical implant layers. Lithographic performance, focusing on CD control over topography and through-pitch behavior, demonstrated the inherent benefit of the DBARCs over the alternative solutions. Small-space residue testing showed the benefit of photosensitive (PS) DBARCs for cleanout of sub-100 nm trenches. A study of improved post-develop residue in various ion-implantation processes validated the use of new DBARC materials in implant layers.

Keywords: DBARCs, photosensitive, implant, KrF, developer-soluble, photoresists, residue, topography

1. INTRODUCTION

Throughout the life of the integrated circuit (IC) industry, developer-soluble bottom anti-reflective coatings (DBARCs) have become familiar. Early DBARCs were a staple for traditional lithography processes. However, as the industry grew, limitations were found with the DBARCs that drove the need for other BARC materials, such as dry BARCs. DBARCs were used for non-critical processes, and dry BARCs were used in critical layers. Nonetheless, in recent years the design rules have once again changed¹. Lithographic processes that were once easily obtained with a single layer of photoresist or top anti-reflective coating (TARC) with photoresist could no longer meet the shrinking critical dimension (CD) requirements. Alternatively, a typical dry BARC could meet the CD requirements, but the substrates were not able to withstand damage from the plasma etching required to remove the dry BARC. In order to meet the demand, a new generation of DBARC materials was introduced for incorporation into the critical implant layers.

As the IC industry realized the need for DBARCs, integration led to challenges. When DBARCs moved into production, it was found that organic residue remained after development, particularly on substrates containing small spaces. This issue culminated in the stalled implementation of DBARCs. Improvements to the DBARC materials and processing have mitigated residue concerns and have allowed DBARC technology to become the desired solution moving forward.

Traditionally, DBARCs have been wholly developer-soluble systems, exhibiting isotropic development. These systems are being used in more mature implant processes. As applications with more advanced designs move into production, traditional DBARCs may show issues with profiles, post-develop residue, and clearing out from small spaces. These challenges make achieving the necessary through-pitch and topography performance difficult. In response, photosensitive (PS) DBARCs were designed that develop anisotropically. These PS DBARCs maintain CD control while showing improved resolution and minimal bias through pitch. The PS DBARCs also offer enhanced clearing in small spaces and a broader process window than traditional DBARCs. For each system, the chemical properties and inherent behavior result in

major strengths as well as challenges. Knowing these, one can select the proper DBARC for a desired application.

1.1 Non-photosensitive

The first DBARC platform was non-photosensitive and purely developer-soluble. These materials typically consist of a polymer matrix that is insoluble in organic solvents but is soluble in alkaline developer. This type of DBARC dissolves equally in all directions, resulting in isotropic development. While this type of development produces very little residue, undercutting of the profile is a concern. The most common method to control the undercut is to modify the develop rate of the isotropic DBARC, which is usually controlled by the film's bake temperature. This modification allows one to change the isotropic DBARC profile from undercut to footing. Develop time must be taken into consideration. If the develop time is not sufficient, footing of the profile can occur, whereas developing for long periods of time can produce undercut. In order to achieve optimum performance, both bake temperature and develop time must be balanced. This property can also be used to help tune the isotropic DBARC performance to a particular application, making these materials highly flexible. In general, the isotropic DBARC systems work independently of the photoresist and perform well with a variety of photoresists.

1.2 Photosensitive

The second DBARC platform is modeled after chemically amplified photoresists. This system is designed to be soluble only in areas exposed with sufficient radiation, thus exhibiting anisotropic development behavior. A PS DBARC coating typically consists of a crosslinked polymer and a photoacid generator (PAG). As the photoresist is exposed, the PS DBARC coating is also exposed, thus generating acid in the PS DBARC film. The acid in the PS DBARC film cleaves the crosslinked bonds, releasing a base-soluble moiety on the polymer, which allows dissolution in alkaline developer. The PS DBARC is similar to a photoresist in that the post-exposure bake (PEB) is key to its performance. Undercut and footing of the profile can be controlled by the PEB, so the PEB process window for the PS DBARC may be limited much like that for a chemically amplified resist. Small changes in BARC bake temperature have little to no effect on undercut/footing of a PS DBARC. Thus, when a PS DBARC is compared with a non-PS DBARC, it is much less sensitive to BARC bake temperature and develop time. Development of the PS DBARC is almost instantaneous, and once the decrosslinking reaction has taken place there is no further erosion of the PS DBARC in developer. The anisotropic nature also minimizes bias through-pitch, enables lower resolution, and enhances clear-out of small spaces on a substrate.

2. METHODOLOGY

2.1 Chemistry

PS BARC formulations were designed with a polymer containing carboxylic acid moieties combined with a multifunctional crosslinker, PAG, quencher, and industry-acceptable solvents. A commercially available isotropic DBARC formulation was obtained from Brewer Science, Inc., and JSR Micro, Inc. supplied the KrF photoresist, M529Y.

2.2 Film properties

To determine solvent resistance, PS BARC formulations were spin coated onto 100-mm silicon wafers and then baked on a bake plate at the recommended temperature for 60 seconds. Ethyl lactate solvent was puddled on the wafer for 20 seconds, and then spun dry. Film thickness was measured before and after processing. A J.A. Woollam Co. M-2000[®] variable-angle spectroscopic ellipsometer (VASE) was used to determine the optical constants n and k at 248 nm. Contrast curve measurements were performed using 200-mm wafers coated via a TEL Clean Track ACT[®] 8 and baked at 160°C for 60 seconds. Wafers were exposed via open-frame exposure on an ASML 750 scanner. Various post-exposure bakes (PEBs) ranging from 105°-135°C were performed, and then the wafers were developed in 0.26N aqueous tetramethylammonium hydroxide (TMAH) for 45 seconds then rinsed with deionized (DI) water and spun dry. In some cases, JSR photoresist was applied atop the PS BARC layer.

2.3 Lithography modeling

PROLITH version 10.1 from KLA-Tencor was used for all reflectivity simulations.

2.4 Post-develop residue determination

Post-develop residue (PDR) was measured using wafers generated from the contrast curve measurements. Native oxide thickness of the substrate was measured before coating using a M-2000[®] VASE. Once the wafer was coated, the M-2000[®] VASE was used to determine the Cauchy coefficients of the PS BARC film. After exposure and development, the areas within the individual exposed die were measured again via the M-2000[®] VASE. Using the native oxide, Cauchy coefficients, and final thickness, a model was built on the M-2000[®] VASE to calculate the average thickness of any remaining PDR.

2.5 Lithography

All lithographic performance was done using a 248-nm scanner. PS BARC thickness was optimized at 38 nm or 60 nm and JSR photoresist at 200 nm or 220 nm. PS BARC bake was at recommended temperature for 60 seconds. The post-application bake (PAB) for the JSR photoresist was 130°C for 90 seconds. PEB was done at various temperatures ranging from 105°-135°C for 90 seconds, and then the wafers were developed in 0.26N TMAH for 45 seconds, rinsed in DI water, and spun dry. Top-down CD profiles were measured using a Hitachi S9380 CD-SEM. Cross-section micrographs were obtained using a Hitachi S-4300 cross-section SEM. Exposures were done using a TEL Clean Track[™] ACT 8 and ASML 750 scanner (NA = 0.70, 0.6 sigma) using conventional illumination.

3. RESULTS AND DISCUSSION

3.1 Material Development

PS DBARC formulations for KrF application were optimized to work best with a particular photoresist in the same manner as prior PS DBARC systems for ArF². A polymer and crosslinking system was selected with n and k values at 248 nm of 1.91 and 0.45, respectively. Crosslinker loading was adjusted to obtain minimal change in ethyl lactate stripping after curing. PROLITH software was used to determine the best thickness for optimum reflectivity control, as shown in Figure 1. The first-minimum thickness of 38 nm on bare silicon was selected as the basis for formulation optimization.

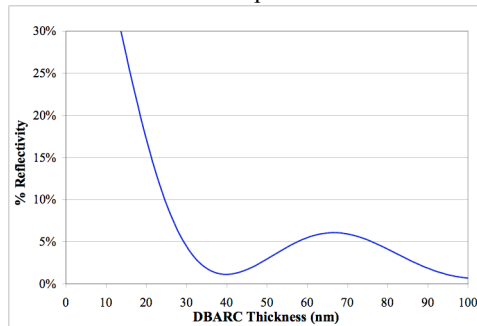


Figure 1. Reflectivity curve on silicon for KrF PS DBARC system.

In order to achieve similar chemical behavior and performance to that of the photoresist, one PAG (PAG 1) and several quenchers (Quenchers 1, 2, and 3) and were selected which closely matched the photogenerated acid and quencher characteristics of the JSR photoresist. Prior work^{3,4,5} with similar PS DBARC systems shows that some photoresists contain PAGs that are capable of diffusing relatively long distances into the DBARC layer. In order to study the behavior of the PAG system in the M529Y photoresist, a PS DBARC formulation was made that contained no PAG and no quencher. Three quenchers were selected to test their effectiveness at quenching potential diffused acid into the PS DBARC. Table 1 shows a summary of the samples.

Table 1. Sample description for quencher selection.

Formulation	Description
A	No PAG / No quencher
B	Quencher 1
C	Quencher 2
D	Quencher 3

The four PS DBARC formulations were coated onto silicon wafers and baked, then the M529Y photoresist was applied and baked and the wafers subjected to contrast curve testing. Figure 2 shows the contrast curve results. Formulation A shows the effect of acid diffusion from the photoresist into the PS DBARC. The M529Y resist generates enough acid to clear the PS DBARC completely. Quencher 2 and 3 are successful at quenching acid from the photoresist, whereas Quencher 1 behaves in an opposite manner by enhancing PS DBARC clearance.

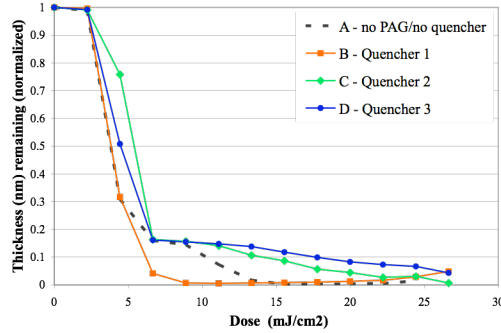


Figure 2. Contrast curve results for initial screening.

From the quencher screening, Quencher 2 and 3 can be considered similar. Quencher 2 most closely matched the quencher system of the M529Y resist, so it was selected for further optimization.

3.2 Formulation optimization

Once a satisfactory quencher had been selected, a formulation matrix was run by varying the PAG and quencher loadings. Details for the design matrix are in Table 2. Lithography was evaluated using the M529Y photoresist. For screening purposes, target CD was set at 170 nm. Dense and isolated trenches were evaluated first.

Table 2. Formulation details for design matrix.

Sample	PAG	Quencher	Exposure Latitude (%)	DOF
1	High	Low	0	0
2	Medium	Low	0	0
3	None	Low	0	0
4	Medium	Medium	13	0.3
5	High	High	0	0
6	Medium	High	18	0.4
7	None	High	17	0.6

The samples containing low amounts of quencher (Samples 1, 2, and 3) had line collapse and no exposure latitude (EL) or depth of focus (DOF). Failure was most likely due to an insufficient quantity of quencher to counteract excessive acid, allowing stray acid to diffuse into unexposed areas. The stray acid from the resist caused decrosslinking of the film in the unexposed areas and undercut of the feature, even in the sample containing no PAG.

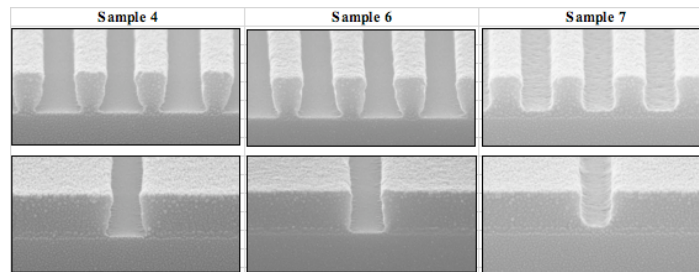


Figure 3. Cross-section results (170S/340P and 170S) for design matrix.

In the remaining samples, at higher quencher levels, a threshold is reached where PAG loading is the controlling factor for line collapse. Figure 3 shows cross sections after lithography with Samples 5, 6, and

7. As the PAG loading changes, the PS DBARC film behavior changes from line collapse in Sample 5 (highest PAG level) to scumming in Sample 7 (no PAG). The medium PAG level (Sample 6) gave clean isolated trenches at the same dose and feature size as the dense spaces. Sample 4 has the same PAG level as Sample 6, but a reduced quencher loading. The dense features for Sample 4 only had 5 nm more undercut than Sample 6. However, the exposure latitude (EL) and DOF for the sample suffered, as a result of increased undercut towards the limits of the process window.

Table 4. Details for additional formulations.

Sample	PAG	Quencher	Exposure Latitude (%)	DOF
8	Low	Med	14	0.6
9	Low	High + 25%	14	0.4
10	Medium	High + 25%	14	0.4

From the first round of testing, Sample 6 performed well, however, the tapered profile can result in poor transfer during the implantation^{6,7,8}. Therefore, straighter sidewalls were desired. Based on the learning from the first design matrix, three additional formulations were tested to find better balance between undercut/line collapse and scumming in the dense and isolated features (Table 4). Figure 4 shows that Sample 8 had the straightest profile.

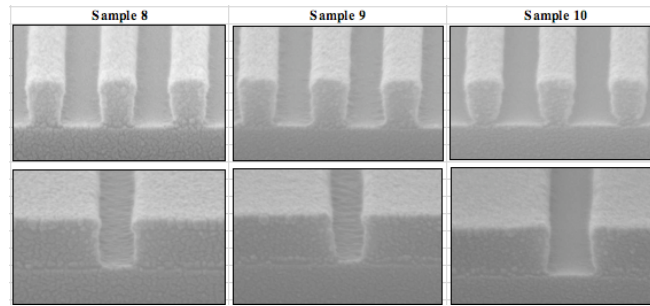


Figure 4. Cross-section results (170S/340P and 170S) for expanded formulations.

3.3 Lithography evaluation

Using the optimized formulation, bright-field isolated and dense features were patterned using formulations from the previous evaluation that gave appreciable EL and DOF of the dark field.

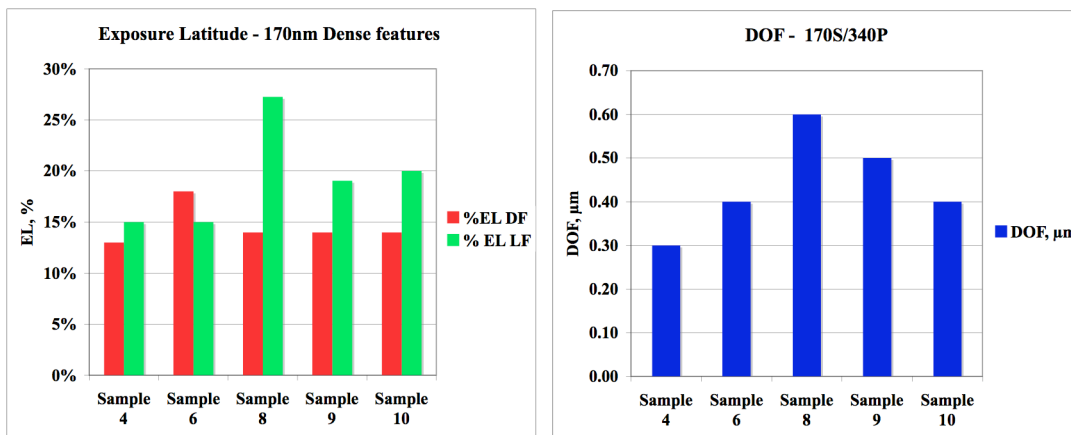


Figure 5. Exposure latitude and DOF comparison for bright-field and dark-field features.

From the DOF and EL data, Sample 8 had the best EL and DOF. Figure 6 shows the cross sections and mask bias required. For all samples, the isolated space had 10-nm gap of the mask while the bright-field line required 80-nm biasing to achieve target CD. The samples containing higher levels of PAG displayed more undercut of the isolated line and tapering of the profiles. The lower PAG levels (Samples 8 and 9)

had less undercut of the isolated line and straight profiles. Based on EL, DOF, and profile shape, Sample 8 was selected for further evaluation.

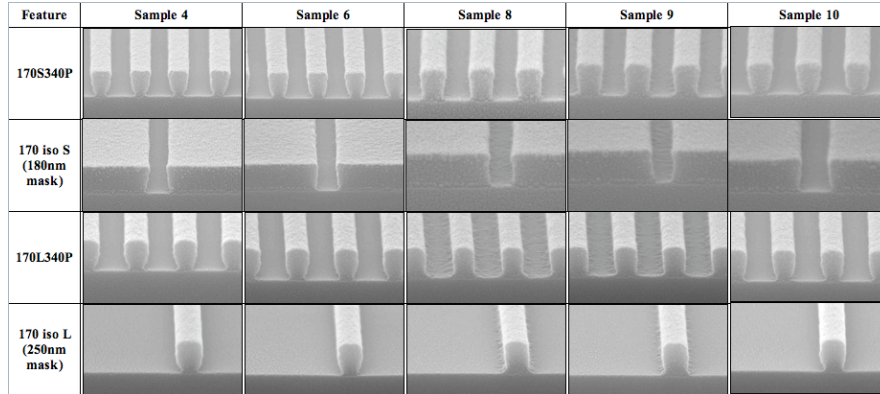


Figure 6. Data through pitch for PS DBARC samples.

3.4 Lithography optimization

As Sample 8 showed promise for the most robust performance, further process modification was needed to achieve the best possible combination of conditions to reduce residue and maximize the process window. First, to find the process conditions that have an effect on residue, a bake matrix combining PS DBARC bake with PEB was done using the M529Y photoresist. Table 5 shows that for all conditions that gave standing features, DOF and EL are greater than 10% and 0.4 μm , respectively. As PS DBARC bake temperature decreases, EL decreases to an average of 14.7%.

Table 5. Bake matrix results, DOF, and EL for 170S340P.

EL (%)					DOF (μm)				
DBARC bake ($^{\circ}\text{C}/60\text{ s}$)	PEB ($^{\circ}\text{C}/90\text{ s}$)				DBARC bake ($^{\circ}\text{C}/60\text{ s}$)	PEB ($^{\circ}\text{C}/90\text{ s}$)			
	120 $^{\circ}\text{C}$	125 $^{\circ}\text{C}$	130 $^{\circ}\text{C}$	135 $^{\circ}\text{C}$		120 $^{\circ}\text{C}$	125 $^{\circ}\text{C}$	130 $^{\circ}\text{C}$	135 $^{\circ}\text{C}$
180 $^{\circ}\text{C}$		10	19	15	180 $^{\circ}\text{C}$		0.5	0.5	0.5
190 $^{\circ}\text{C}$		15	15		190 $^{\circ}\text{C}$		0.4	0.6	
200 $^{\circ}\text{C}$	20	20			200 $^{\circ}\text{C}$	0.6	0.5		
210 $^{\circ}\text{C}$	19	19			210 $^{\circ}\text{C}$	0.6	0.4		
220 $^{\circ}\text{C}$	19				220 $^{\circ}\text{C}$	0.5			

The limiting factor for performance, residue between the lines, is shown in Figure 7 with cross-section data for the dense 170-nm trenches. At PS DBARC bake temperatures above 200 $^{\circ}\text{C}$, post-develop residue is minimized. Below a 200 $^{\circ}\text{C}$ bake, post-develop residue increases, but it can be mitigated by adjusting the PEB. In order to have an equivalent amount of residue at 180 $^{\circ}\text{C}$ compared to 200 $^{\circ}\text{C}$, an increase of 10 $^{\circ}\text{C}$ was required.

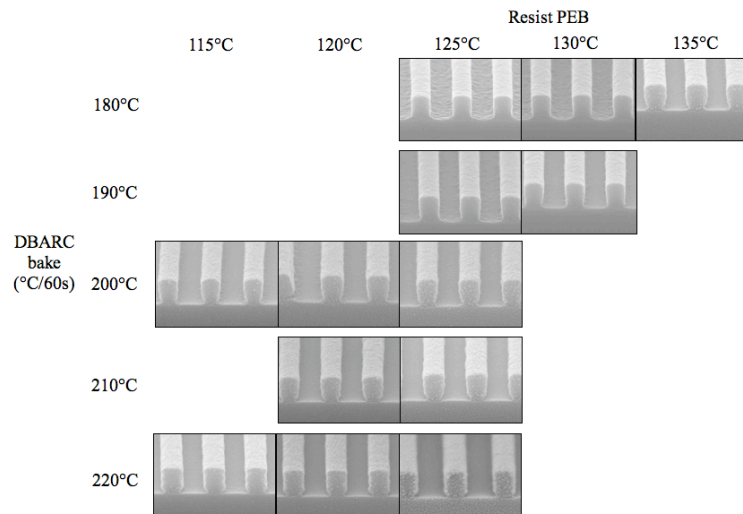


Figure 7. Cross-section data for 170S340P features, through PS DBARC bake and PEB.

Figure 8 shows the full comparison through pitch for the 200°C PS DBARC bake coupled with the 125°C PEB. The mask was biased for the isolated features. The trench was biased at a mask size of 220 nm, and the isolated line was biased at 250 nm. Overlapping DOF for all features was 0.5 μm . At these conditions, residue of all features was minimized.

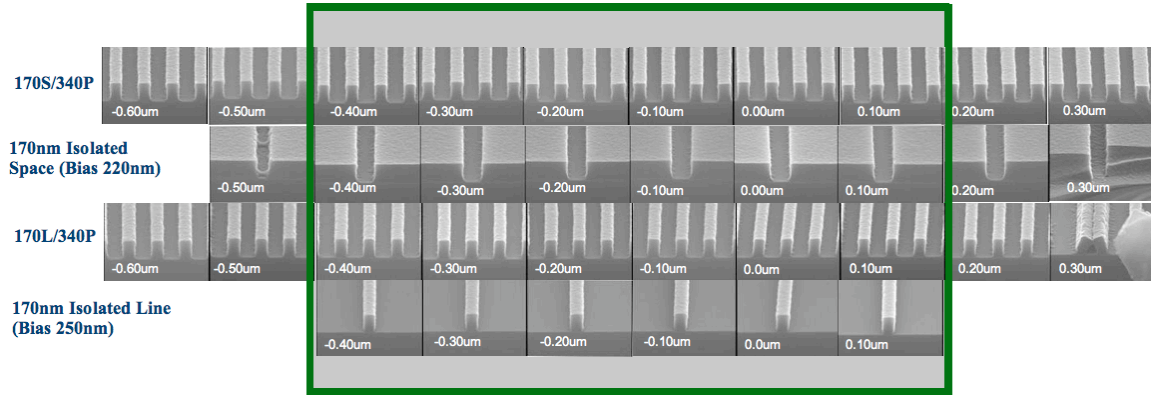


Figure 8. Overlapping DOF for optimized process conditions at 170-nm features.

3.5 Residue Data

After the lithography process was optimized, characterization of the residue after development was tested. Figure 9 shows the post-develop residue comparison for various materials. The resist, isotropic DBARC, and PS DBARC all have less than 1 nm of residue remaining after development.

Clear-out of small spaces is also an area of concern for implant processes. Due to underlying topography in implant applications, there was concern that the develop process would not be sufficient to remove the DBARCs completely from the small areas. Before the DBARCs were incorporated on a topography substrate, clear-out in a small trench was tested to ensure residue would not remain after patterning. Trench dimensions were 100 nm deep and 80 nm wide. A blank wafer was tested against wafers coated with DBARC and photoresist, then exposed, subjected to a PEB, and developed. Figure 10 shows results for the clear-out testing. Both of the DBARC materials showed little residue remaining in the trenches.

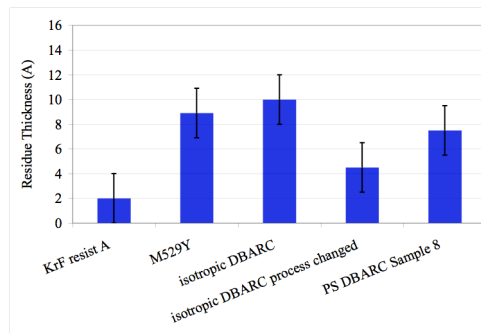


Figure 9. Post-develop residue values for various materials.

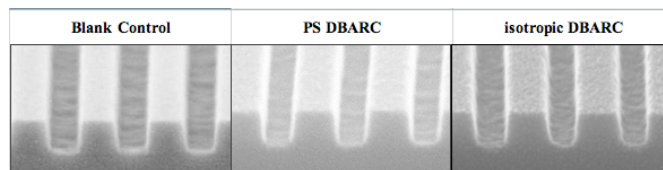


Figure 10. Small space clear-out of DBARCs showing minimal residue remaining.

3.6 Lithography over topography

In a typical implant application, the implant blocking layer will be coated on a substrate with underlying features with changes in step height and width. The advantage of using a BARC to control changes in CD

as photoresist is coated over existing topography is well known^{9,10,11}. The BARC provides optimum reflectivity control over substrates as composition changes and as the photoresist thickness adjusts over topography. The benefit of the DBARC concept was tested against a photoresist/TARC combination by printing lines on top of 110-nm silicon dioxide trenches. Top-down images were measured via CD-SEM.

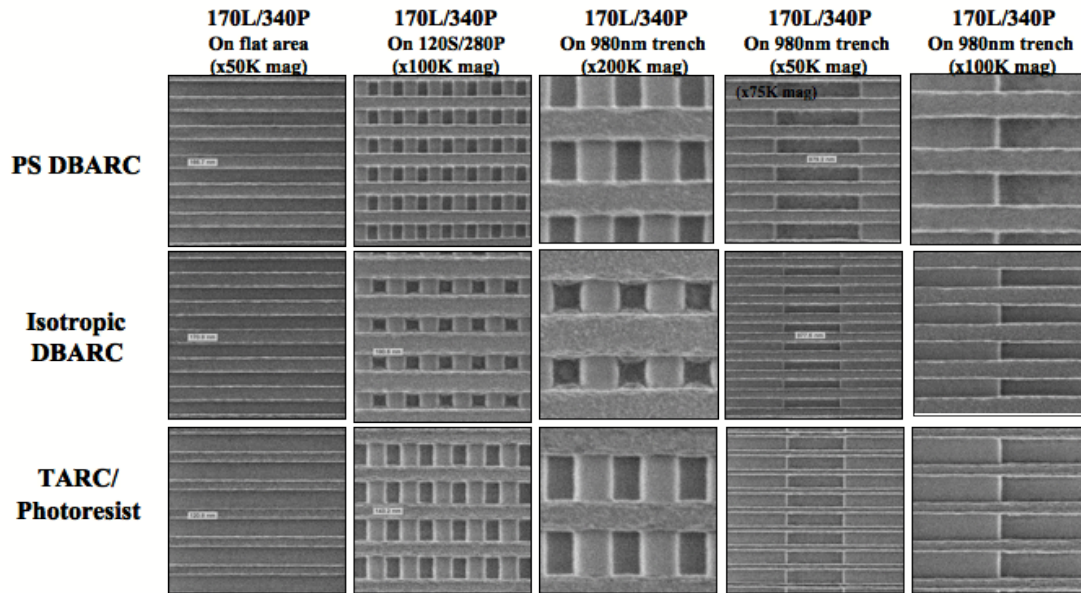


Figure 11. Top-down CD-SEM results over 110 nm deep SiO₂ topography.

For all three combinations, initial profiles in Figure 11 look promising. However, after examination of the dense patterns, the isotropic DBARC had residue present in the small spaces. The PS DBARC and TARC had clean dense spaces. Critical dimension of semi-dense lines was measured on top of a step 500 nm wide and in the adjacent open area 1 micron wide. Table 6 shows results for the change in CD as the thickness of the photoresist changes over the step. Top-down CD was measured in the open space of a trench and compared to the CD on top of an adjoining step. While the TARC/photoresist leaves no residue in the small spaces, the change in CD as the lines are formed over topography is 35%. The two DBARCs give better results; both give 10% to 15% change in CD.

Table 6. Data showing change in CD over various topography heights.

CD Change over step			
System	CD (nm) open area	CD (nm) top of trench	% change
TARC	230	150	34.8
isotropic DBARC	190	160	15.8
PS DBARC	180	160	11.1

3.7 Ion implantation evaluation

The final round of testing was to determine if the residue remaining after develop would interfere with the final ion implantation. Silicon wafers with 10 nm of silicon dioxide were coated with the various DBARCs or resist. Some samples were implanted without further processing to simulate the unexposed areas of the film. A second set of wafers were exposed at a dose to give the same amount of residue as in Figure 8, subjected to PEB, and then developed. Once processing was complete, wafer samples were implanted with boron at low implant energies of 5 KeV and 21 KeV. The dose was varied at either $3 \times 10^{14}/\text{cm}^2$ or $5 \times 10^{14}/\text{cm}^2$. Secondary mass ion spectroscopy (SIMS) was used to measure the boron depth profile and concentration. Data for peak concentration and depth are shown in Figures 12a and 12b. At the low energy/low dose, implantation was done in two runs. The first run was through the residues of the exposed photoresist and the isotropic DBARC/photoresist. The second run included the PS DBARC/photoresist system. Peak concentration (C_p) for all three systems is similar to the non-coated control wafer. However, peak depth varied up to 7% from the control. A second test was run at 21 KeV using the photoresist and

isotropic DBARC/photoresist. A non-exposed photoresist sample was also included. At higher energies, the implant depth and concentration are more consistent. For this implant, any residues remaining after exposure did not interfere with the ion implantation depth.

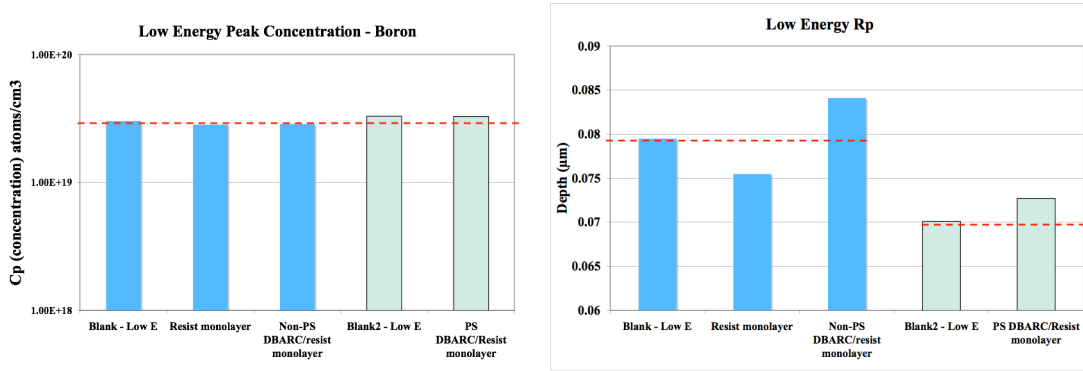


Figure 12a. Low-energy implantation data through residue.

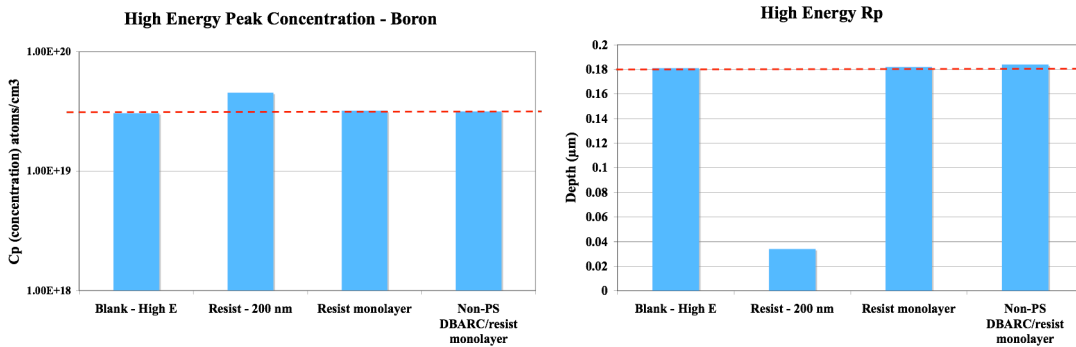


Figure 12b. High-energy implantation through residue.

Further investigation was done to determine if the DBARCs exhibited any ion blocking characteristics. Similar tests were run as before, at high and low energy/dose. However, the coated films were not exposed prior to implantation. Data for peak concentration and depth are shown in Figures 13a and 13b. At low energy/dose, the photoresist was 100% effective at blocking any ion penetration into the substrate. The DBARCs were coated without covering photoresist. At 38-40 nm of film thickness, both materials reduced ion penetration into the substrate by almost 50%. At high energy/dose, the addition of the DBARC to the resist reduced implantation depth by 37%. Unfortunately, at the higher conditions, the DBARC alone did not offer as much blocking ability as at the lower conditions. Only 10% of the implant was blocked.

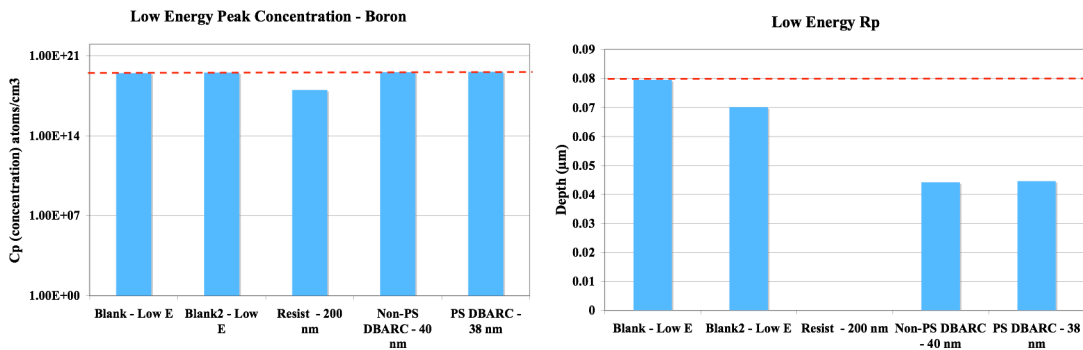


Figure 13a. Low-energy implant blocking data.

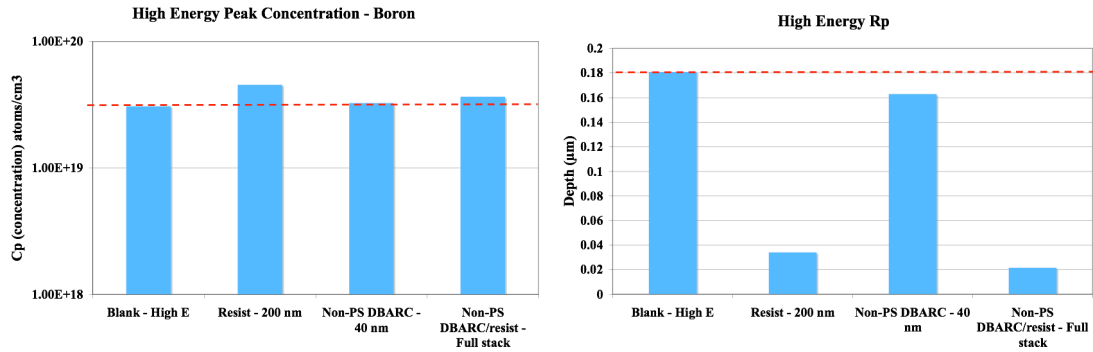


Figure 13b. High-energy implant blocking data.

4. CONCLUSIONS

As DBARC systems become more common in critical processes, they will need to fulfill a variety of requirements in order to meet the rigorous demands essential to their success. Selection of an optimal photoresist/DBARC combination is key for development speed and best overall performance, and developing the materials to work jointly as a system is vital. Lithographic performance, focusing on CD control over topography and through-pitch behavior, demonstrates the inherent benefit of DBARC over the alternative solutions. Process optimization allows the DBARC to be tuned for incorporation into an IC manufacturer's device. Study of improved post-develop residue in various ion-implantation processes validates the use of new DBARC materials in implant layers. As features shrink and more engineers begin using or increase their use of DBARCs, proving the feasibility of the technology by working together with IC device manufacturers will become vital for successful execution.

REFERENCES

- [1] Lee, H.-R., Popova, I. Y., Rolick, J. M., Gomez, J.-M., and Bailey, T. C., "Message to the undecided – Using DUV dBARC for 32 nm node implants," *Proc. SPIE 7273*, 72730Y (2009).
- [2] Lowes, J., Pham, V., Meador, J., Stroud, C., Rosas, F., Mercado, R.-M., Slezak, M., "Advantages of BARC and photoresist matching for 193-nm photosensitive BARC applications," *Proc. SPIE 7639*, 76390K-1 (2010).
- [3] Meador, J., Guerrero, A., Lowes, J., Stroud, C., Carr, B., Qin, A., Washburn, C., Mercado, R.-M., "Photoresist-induced development behavior in DBARCs," *Proc. SPIE 7639*, 763926-1 (2010).
- [4] Wallraff, G., Larson, C., Fender, N., Davis, B., Medeiros, D., Meute, J., "Characterization and Acid Diffusion Measurements of New Strong Acid Photoacid Generators," *Proc. SPIE 4690*, 161-167 (2002).
- [5] Utsumi, Y., Komuro, Y., Kawae, A., Seshimo, T., Hada, H., Nakamura, T., Yoshii, Y., Onodera, J., Ogawa, S., "Study of PAG Material Design for ArF Immersion Photoresist," *Journal of Photopolymer Science and Technology* 21(6), 719-723 (2008).
- [6] Bailey, T., McIntyre, G., Zhang, B., Deschner, R., Mehta, S., Song, W., Lee, H.-R., Hu, Y., Brodsky, M., "Reflectivity-induced Variation in Implant Layer Lithography," *Proc. SPIE 6924*, 69244F-1 (2008).
- [7] Gulimeau, I., Guerrero, A., Blain, V., Kremer, S., Vachellerie, V., Lenoble, D., Nogueira, P., Mougel, S., Chapon, J.-D., "Evaluation of wet-developable KrF organic BARC to improve CD uniformity for implant application," *Proc. SPIE 5376*, 461-470 (2004).
- [8] Grandpierre, A., Berger, C., Schroeder, U., Schiwon, R., Kubis, M., "Comparison of I-line and DUV high energy implant litho processes," *Proc. SPIE 6512*, 61523V-1 (2006).
- [9] Cameron, J., Amara, J., Sung, J. W., Valeri, D., Ware, A., O'Shea, K., Yamamoto, Y., Kitaguchi, H., Vyklicky, L., Popova, I., Varanasi, P. R., "Design and Development of Developable BARCs (DBARCs) for Advanced Lithographic Applications," *Journal of Photopolymer Science and Technology* 23(5), 721-729 (2010).
- [10] Owe-Yang, D. C., Ho, B.-C., Miyazaki, S., Katayama, T., Susukida, K., Kang, W., Chang, Y.-C., "Application of photosensitive BARC and KrF resist on implant layers," *Proc. SPIE 5376*, 452-460 (2004).

[11] Washburn, C., Mercado, R., Guerrero, D., Meador, J., "Controlling CD and process window limits for implant patterning," *Solid State Technology* 49(10), 53-56 (2006).